

Application of Adaptive Time-Stepping for Steady/Unsteady Flows

Nikhil Kalkote*, Ashwani Assam* and Vinayak Eswaran*,**

**Corresponding author: eswar@iith.ac.in

* PhD Student

** Professor

Department of Mechanical and Aerospace Engineering,
Indian Institute of Technology Hyderabad, India.

1 Abstract

Adaptive time-stepping is a method of choosing a variable time-step size for time-marching applications given prescribed tolerance for local error. When applied to steady-state problems this method acts as a convergence accelerator while for transient problems it maintains the time accuracy using a user-prescribed error criterion. In this paper, we demonstrate the usefulness of this method over the commonly-used CFL based time-stepping for different problems with steady/unsteady laminar viscous flow.

2 Introduction

Time-step size in CFD simulations is generally determined from the CFL condition, which ensures numerical stability if explicit marching is used. The same method is used even in implicit scheme, where time-step size is not restricted by the stability condition, by using an empirically chosen CFL number based on past experience. In the steady-state problems, the use of large CFL is recommended as it mitigates the dependence of the convergence to the steady-state on (arbitrarily) initial conditions[1]. This is generally achieved by ramping up the CFL number as the solution proceeds. The lower, upper bound and optimal rate of increase changes from problem to problem and is generally decided by past experience, still does not ensure the boundedness of the solution which may "blow-up". It would therefore be useful to have a closed loop algorithm for time-stepping that ensures boundedness/stability when increasing the CFL numbers.

In this paper we demonstrate the usefulness of adaptive time-stepping based on local-error control previously used extensively in ODE integration. The idea of choosing a time-step size based on local error is an old idea in numerical analysis, after being popularised by Gear [2, 3, 4], Greenspan [5] and Morrison [6] in the 1960s. Since then this method has extensively used to handle the stiff ODEs, but not so much in numerical solution of PDEs in CFD. The use of adaptive time-stepping (ATS) with local truncation error control enables the solver to use the maximum allowable time-step, for the prescribed tolerance of error. The algorithm is also capable of converging very rapidly to the steady state (if there is any) after the initial transient phase, i.e in later convergence. We present here only the first order time-stepping scheme. However method is extendable to sixth-order. While the order of the scheme does not affect the accuracy, because of the local error control, higher order solutions may prove to be more efficient.

3 Governing Differential Equation

The integral form of the compressible Navier-Stokes equation for an arbitrary control volume V with an elemental surface area $d\vec{A}$ with outward unit normal $\mathbf{n} = (n_x, n_y, n_z)$ is written as:

$$\underline{\Gamma} \int \frac{\partial}{\partial t} \mathbf{Q} dV + \int [\mathbf{F} - \mathbf{G}] dA - \int \mathbf{S} dV = 0 \quad (1)$$

where \mathbf{Q} is the vector of primitive variables, \mathbf{F} , \mathbf{G} are the normal components of the convective and viscous flux vectors at the elemental surface, \mathbf{S} is the vector of source terms and Γ is the transformation Jacobian of the conservative variables with respect to primitive variables at cell p . These quantities are given by:

$$\mathbf{F} = \begin{pmatrix} \rho V_n \\ \rho V_n u + P n_x \\ \rho V_n v + P n_y \\ \rho V_n w + P n_z \\ \rho V_n H \end{pmatrix} \quad \mathbf{G} = \begin{pmatrix} 0 \\ n_x \tau_{xx} + n_y \tau_{xy} + n_z \tau_{xz} \\ n_x \tau_{yx} + n_y \tau_{yy} + n_z \tau_{yz} \\ n_x \tau_{zx} + n_y \tau_{zy} + n_z \tau_{zz} \\ n_x \theta_x + n_y \theta_y + n_z \theta_z \end{pmatrix} \quad \mathbf{S} = \begin{pmatrix} 0 \\ \rho f_x \\ \rho f_y \\ \rho f_z \\ \rho(f_x u + f_y v + f_z w) + \dot{q}_h \end{pmatrix} \quad (2)$$

where f_x, f_y and f_z are external body forces per unit mass, \dot{q}_h is the volumetric heating rate, P is the pressure, H is the total enthalpy and the primitive variable vector is

$$\mathbf{Q}^T = (P \quad u \quad v \quad w \quad T)$$

$V_n, \theta_x, \theta_y, \theta_z$ and the matrix Γ are given by [7]:

$$\begin{aligned} V_n &= n_x u + n_y v + n_z w \\ \theta_x &= u \tau_{xx} + v \tau_{xy} + w \tau_{xz} + k \frac{\partial T}{\partial x} \\ \theta_y &= u \tau_{yx} + v \tau_{yy} + w \tau_{yz} + k \frac{\partial T}{\partial y} \\ \theta_z &= u \tau_{zx} + v \tau_{zy} + w \tau_{zz} + k \frac{\partial T}{\partial z} \end{aligned} \quad \underline{\Gamma} = \begin{bmatrix} \rho_p & 0 & 0 & 0 & \rho T \\ u \rho_p & \rho & 0 & 0 & u \rho T \\ v \rho_p & 0 & \rho & 0 & v \rho T \\ w \rho_p & 0 & 0 & \rho & w \rho T \\ H \rho_p - 1 & u \rho & v \rho & w \rho & \rho T H + \rho C_p \end{bmatrix}$$

where subscripts (except in C_p) indicate differentiation with respect to the subscripting variable. The system is closed using the equation of state $P = \rho R T$.

Using the Gauss divergence theorem, equation (1) is discretized for a general multi-face cell as,

$$\underline{\Gamma} \frac{\partial}{\partial t} \mathbf{Q} + \sum_f (\mathbf{F}_f - \mathbf{G}_f)^{n+1} A_f - \mathbf{S}^{n+1} V = 0 \quad (3)$$

where f refers to the faces of the cell.

4 Implicit Time Integration

In the semi-discretized governing equations above, the values of the fluxes \mathbf{F} , \mathbf{G} are not known at the $n+1$ level. Expanding the global residual vector $\mathbf{R}^{n+1} (\equiv \mathbf{F}^{n+1} - \mathbf{G}^{n+1} - \mathbf{S}^{n+1})$, around the known residual flux \mathbf{R}^n , we get

$$\mathbf{R}^{n+1} = \mathbf{R}^n + \left(\frac{\partial \mathbf{R}}{\partial \mathbf{Q}} \right)^n \Delta \mathbf{Q}^{n+1} + \text{H.O.T} \quad (4)$$

where $\Delta \mathbf{Q}^{n+1} = \mathbf{Q}^{n+1} - \mathbf{Q}^n$, and the quantity in brackets is the Jacobian. With (4), the system (3) results in:

$$\left[\frac{V_p}{\Delta t} \underline{\Gamma} + \sum_f J_{f,p} A_f \right] \Delta \mathbf{Q}_p^{n+1} - \sum_f J_{f,nb} \Delta \mathbf{Q}_{nb}^{n+1} = -\mathbf{R}^n \quad (5)$$

where p, nb refers to centres of the cell and its neighbours, respectively, V_p is the p^{th} cell volume, $\underline{J}_{f,p/nb}$ is the *flux* Jacobian matrix of the discretized flux ($\mathbf{F}^n - \mathbf{G}^n - \mathbf{S}^n$) with respect to variables at the p or nb cell-centres. The discretized flux at face f is a function of the p^{th} cell value as well as the neighbouring cell values, thus the neighbouring nb term appears in the equation above. Rearranging equation (5), we get

$$[\underline{I} - \Sigma_f \underline{J}_{j,nb} A_f] \Delta \mathbf{Q}^{n+1} = -\mathbf{R}^n \quad \text{or} \quad [\underline{A}]_{global} \Delta \mathbf{Q}^{n+1} = -\mathbf{R}^n \quad (6)$$

where

$$\underline{I} \equiv \left[\frac{V}{\Delta t} \underline{\Gamma} + \Sigma_f \underline{J}_{f,p} A_f \right] \quad (7)$$

and $\Delta \mathbf{Q}$ now includes the values at p and nb , in fact all points of the domain. The equation set (6) is solved using the symmetric Gauss-Seidal procedure [8, 9].

4.0.1 Quadratic convergence at large time-steps

In the discretized Navier-Stokes equation (6), larger time-steps Δt reduce the contribution from the temporal term. Thus for large time-steps, the system of equations (6) reduces to Newton's root-finding method for the steady-state problem which has quadratic convergence. However, the direct use of large time-steps without local error control is not a good strategy, neither during initial convergence nor for later-convergence. In the former case, the large Δt applied to a developing solution creates large errors causing delayed convergence. In the latter case, a bounded solution is not ensured due to uncontrolled local error and the solution may diverge. In this paper we have used CFL based time-stepping during initial convergence (defined as any residuals of (5) greater than 10^{-2}) and adaptive time-stepping for later-convergence (all residuals below 10^{-3}).

5 All speed algorithm

When compressible methods are applied to low Mach number flows, care has to be taken to deal with the stiffness associated with large condition numbers, otherwise, density-based algorithms will not converge for low-Mach-number or incompressible flow problems. One way to handle this is by preconditioning of the time-derivative [10, 11, 9]. But this destroys the time-accuracy thus requires unsteady problems to be solved as a series of pseudo-steady problems which is computationally expensive. Shima and Kitamura [12, 13] have proposed an algorithm called SLAU (Simple Low dissipation AUSM) to deal with this problem which does not rely on preconditioning of the time-derivative. We use this method for all-speed applications. The step-by-step algorithm to discretize convective flux follows Shima et al. [14].

6 Results and Discussions

The compressible Navier-Stokes equations has been solved using a density-based algorithm in the framework of our in-house 3D unstructured solver. This solver was previously tested for various Mach number regimes of steady state flow [15, 16, 17]. Here, an all speed SLAU [18] scheme is used for the convection and the Green-Gauss[7] method is used for diffusion term discretization. The convective term uses second-order discretization while the viscous term are central discretized [7]. The first-order backward Euler method is used for time-stepping [19]. Although the method is only first-order, this does not affect the accuracy of the solution, which is fixed by the user-prescribed error tolerance. Its feature of capturing unsteadiness in the flow for transient problems and as a later-convergence accelerator for steady-state problem is shown below for two different cases.

6.1 Laminar Flow over a NACA 0012 Aerofoil

Swanson and Langer [20] have presented a detailed documentation for two cases, which we use to demonstrate the advantages of ATS over the CFL-based time-stepping method. The cases are tabulated in Table 1. The Reynolds number is calculated based on the unit chord-length of the airfoil. The far-field boundary in the

grid is located almost 500 chord-lengths away from the airfoil in order to minimize the sensitivity to far-field. The flow domain and boundary conditions applied are shown in Fig. 1. The CFL number used for the CFL based time-stepping is taken as 200.

Table 1: Cases considered.

Cases	M_∞	α (deg.)	Re_c
Case 1	0.5	0.0	5×10^3
Case 2	0.5	3.0	5×10^3

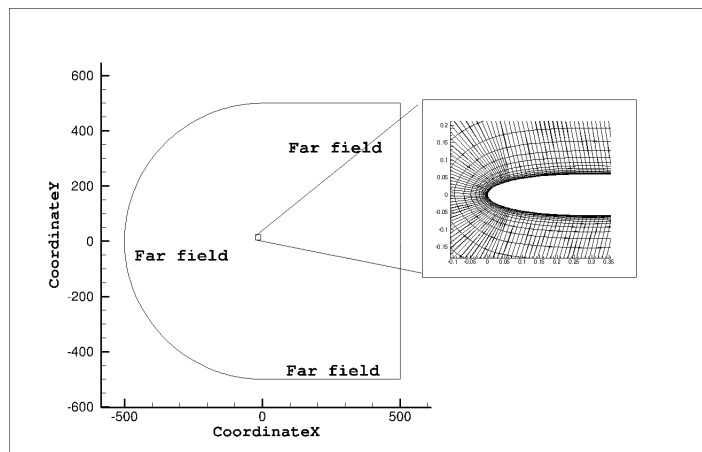


Figure 1: Flow domain for turbulent flow over NACA 0012 airfoil with a zoomed view of the nose of the airfoil.

The results for skin friction coefficient (C_f) are matched with CFD results presented in the reference [20]. Figure 2 shows the C_f plot along the surface of the airfoil for $\alpha = 0^\circ$ and 3° computed using both the time-stepping methods. Both (ATS and CFL based) time-stepping methods give accurate results in comparison with the reference solution and themselves are nearly identical. Figure 3 shows the residual plot of the flow variables for CFL based time-stepping. It can be seen that the residuals for flow variables shows a gradual drop before stalling at a value of around 10^{-6} for both the angles of attack (α). For $\alpha = 0^\circ$ the stalling occurred after around 800 iterations while for $\alpha = 3^\circ$ the stalling occurred after 2000 iterations. Figure 4 shows the comparison of the convergence history of the CFL based time-stepping with the ATS method. We see a marked reduction in the number of iteration required for the convergence, as the ATS method gave convergence to machine precision 10^{-15} (in comparison to the CFL based method which stalled at 10^{-6}) in only 290 and 350 iteration for the two cases, respectively. The speed-up of 275.86% and 769.23% due to ATS w.r.t CFL based time-stepping respectively for $\alpha = 0^\circ$ and 3° , shows the effectiveness of the ATS.

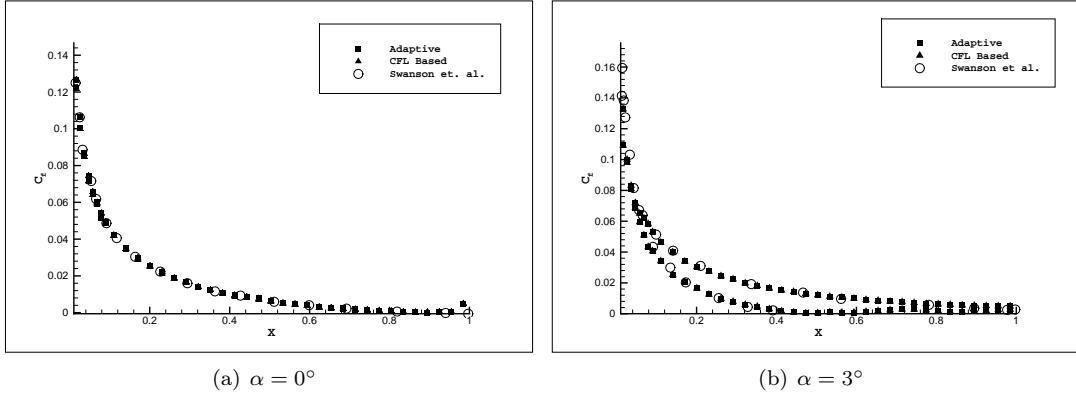


Figure 2: Skin friction Coefficient (C_f) for the two cases considered. The results are compared with the reference solution of Swanson and Langer [20].

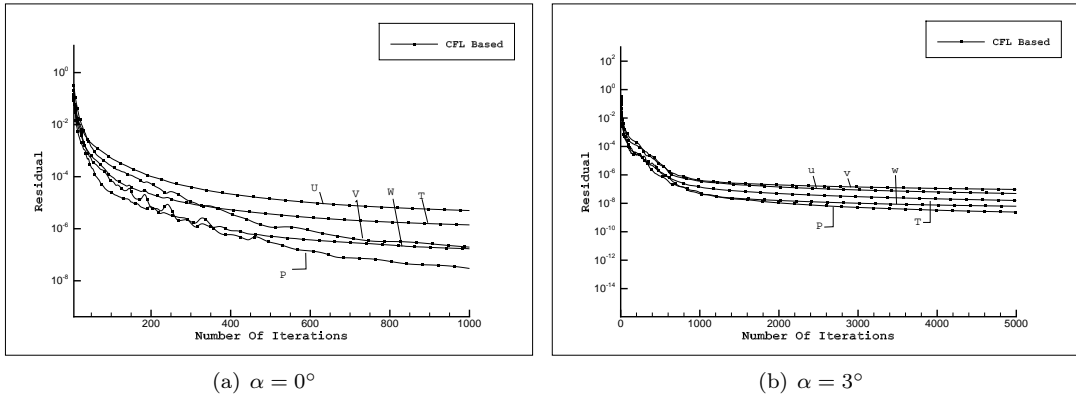


Figure 3: Convergence history of scaled residue with a CFL based time-stepping for Case 1 & 2: The residuals stalled around 10^{-6} for both the angles of attack (α) after around 800 and 2000 iterations respectively.

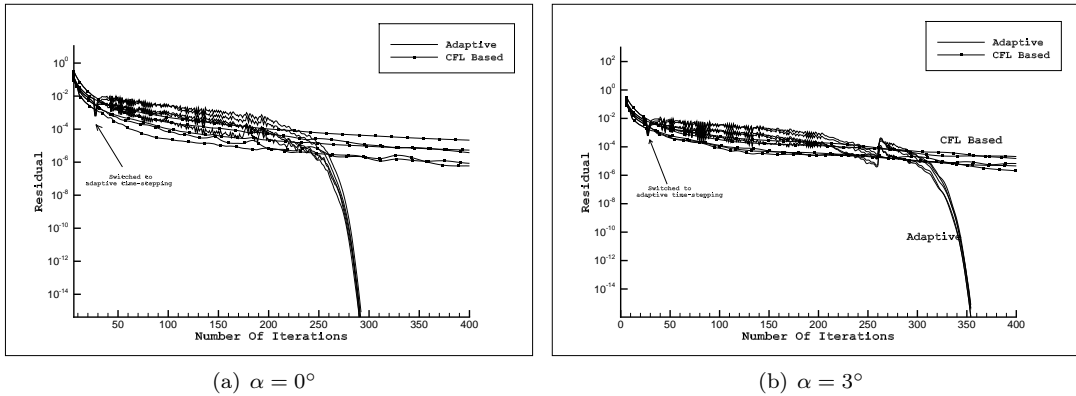


Figure 4: History of later-convergence with adaptive time-stepping for both the angles of attack (α) for Case 1 & 2. Adaptive time-stepping (ATS) took around 290 and 350 iterations respectively in the later-convergence to reach machine precision (residual value of $< 10^{-15}$).

	Present work	Rajani et al. [26]	Williamson & Roshiko [29]	Norberg C. [23]
Amplitude of lift coefficient	0.282	0.26	-	-
Strouhal Number	0.156	0.1569	0.154	0.155

Table 2: Comparison of amplitude of lift coefficient and Strouhal number with numerical solution of Rajani et al. [26] for flow over a circular cylinder

6.2 Flow over a circular cylinder

The next problem considered is the unsteady *incompressible* flow past a circular cylinder. Extensive numerical data is available in the literature [24, 25, 26, 27] for this problem for Reynolds number $Re_D = 100$ which is in the regime of laminar 2-D flow with periodic vortex shedding [25]. However as ours is a compressible flow solver, we still need to specify the temperature. The cylinder diameter (D) is taken as 1m and the free-stream temperature and velocity are taken as 300K and $0.1Ma$ which is essentially in the incompressible limit and viscosity is adjusted as per the chosen Reynolds number.

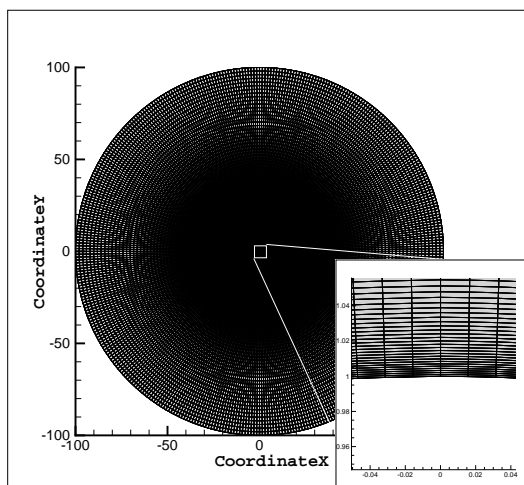


Figure 5: Hex O-grid mesh set-up used for flow the cylinder case.

An O-type grid is used for the mesh and is shown in Fig 5. It has 401 grid points on the cylinder and 201 grid points normal to the cylinder. The grid is generated with a bi-geometric law which is used to distribute points in the normal direction with the initial spacing (near cylinder wall) of 0.001045 diameters and a spacing ratio of 1.15 away from the wall. The far field is located at 100 diameters from the cylinder center. The above mesh set-up is as used by Green et al.[28]. At $Re = 100$ periodic vortex shedding occurs. Fig 6 shows the u -velocity contours at a particular time instant and the periodic variation of lift coefficient (C_l) with time. It can be seen that the periodic vortex shedding is successfully captured qualitatively. The Strouhal number is defined as

$$St = \frac{fL}{U_\infty} \quad (8)$$

where f is the frequency of the vortex shedding, L is the characteristic length and U_∞ is the free-stream velocity. Table 2 compares the amplitude of C_l plotted in the Fig 6 and the Strouhal number with three reference results [29, 23, 26]. The Strouhal number obtained in this computation is 0.156, which compares well with the literature values of 0.1569 [26], 0.154 [29] and 0.155 [23]. The amplitude of the lift coefficient also matches well with that from the literature.

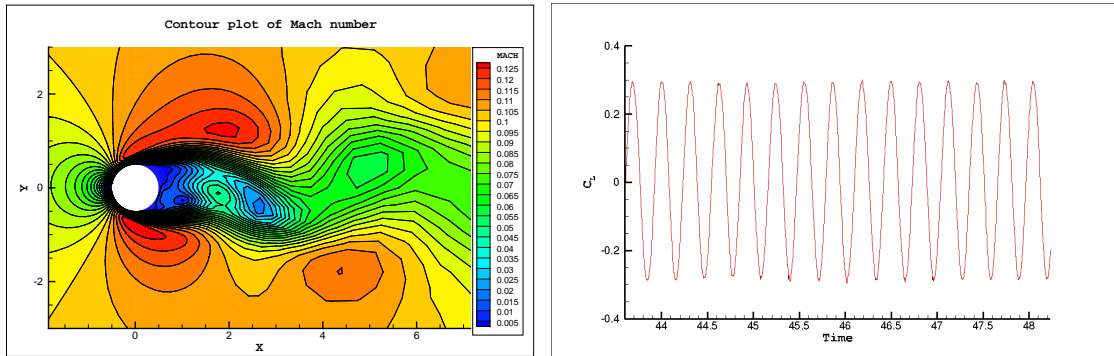


Figure 6: Contour plot of Mach number and the variation of lift coefficient at Re 100 for flow over a circular cylinder.

7 Conclusions

- In the present paper we have demonstrated the effectiveness of adaptive time-stepping (ATS) to accelerate convergence of false transient time-stepping to steady-state solutions of an implicit compressible Navier-Stokes algorithm. The method is used only for later-convergence, after all residuals have been brought below 10^{-2} by first using conventional CFL-based time-stepping. The acceleration obtained is 500-1000% in comparison to CFL based time-stepping.
- We also validate the use the adaptive time-stepping via local error control for unsteady flow computations of 2-D flow over a circular cylinder involving vortex shedding. We see the unsteadiness in the flow is properly captured. The Strouhal number for circular cylinder case is in good agreement with the literature, despite the use of a compressible solver for an incompressible flow problem.

References

- [1] Chenzhou Lian, Guoping Xia, and Charles L. Merkle. Solution-limited time stepping to enhance reliability in cfd applications. *Journal of Computational Physics*, 228(13):4836 – 4857, 2009.
- [2] Charles William Gear. The numerical integration of ordinary differential equations. *Mathematics of Computation*, 21(98):146–156, 1967.
- [3] C William Gear. The automatic integration of ordinary differential equations. *Communications of the ACM*, 14(3):176–179, 1971.
- [4] Robert K Brayton, Fred G Gustavson, and Gary D Hachtel. A new efficient algorithm for solving differential-algebraic systems using implicit backward differentiation formulas. *Proceedings of the IEEE*, 60(1):98–108, 1972.
- [5] H Greenspan, W Hafner, and Marijan Ribarič. On varying stepsize in numerical integration of first order differential equations. *Numerische Mathematik*, 7(4):286–291, 1965.
- [6] D Morrison. Optimal mesh size in the numerical integration of an ordinary differential equation. *Journal of the ACM (JACM)*, 9(1):98–103, 1962.
- [7] J Blazek. *Computational fluid dynamics principles and applications*. Elsevier, Amsterdam; San Diego, 2005.
- [8] Seokkwan Yoon and Antony Jameson. Lower-upper symmetric-gauss-seidel method for the euler and navier-stokes equations. *AIAA Journal*, 26(9):1025–1026, 1988.
- [9] Jonathan M Weiss, Joseph P Maruszewski, and Wayne A Smith. Implicit solution of preconditioned navier-stokes equations using algebraic multigrid. *AIAA Journal*, 37(1):29–36, 1999.
- [10] S Venkateswaran and Charles Merkle. Dual time-stepping and preconditioning for unsteady computations. In *33rd Aerospace Sciences Meeting and Exhibit*, page 78, 1995.
- [11] Jonathan Weiss and Wayne Smith. Preconditioning applied to variable and constant density time-accurate flows on unstructured meshes. In *Fluid Dynamics Conference*, page 2209, 1994.

- [12] Meng-Sing Liou. A sequel to ausm, part ii: Ausm+-up for all speeds. *Journal of Computational Physics*, 214(1):137–170, 2006.
- [13] Eiji Shima and Keiichi Kitamura. On new simple low-dissipation scheme of ausm-family for all speeds. In *47th AIAA Aerospace Sciences Meeting including the New Horizons Forum and Aerospace Exposition*, page 136, 2009.
- [14] Eiji Shima and Keiichi Kitamura. New approaches for computation of low mach number flows. *Computers & Fluids*, 85:143–152, 2013.
- [15] Ashwani Assam, Nikhil Narayan Kalkote, Vatsalya Sharma, and Vinayak Eswaran. An automatic wall treatment for spalart-allmaras turbulence model. *Journal of Fluids Engineering*, 2018.
- [16] Nikhil Kalkote Vinayak Eswaran. Supersonic biplane: Cheaper, quieter and fuel efficient supersonic travel. In *Proceedings of the 6th International and 43rd National Conference on Fluid Mechanics and Fluid Power*, 2016.
- [17] Nikhil Kalkote Vinayak Eswaran. Numerical computation of natural convection on unstructured hybrid mesh without preconditioning. In *24th National and 2nd International ISHMT-ASTFE Heat and Mass Transfer Conference*, 2017.
- [18] Eiji Shima and Keiichi Kitamura. Parameter-free simple low-dissipation ausm-family scheme for all speeds. *AIAA journal*, 49(8):1693–1709, 2011.
- [19] Nikhil Kalkote Vinayak Eswaran. Unsteady computations of all speed flows with modified gear’s method on unstructured hybrid grid. In *24th National and 2nd International ISHMT-ASTFE Heat and Mass Transfer Conference*, 2017.
- [20] RC Swanson and Stefan Langer. Steady-state laminar flow solutions for naca 0012 airfoil. *Computers & Fluids*, 126:102–128, 2016.
- [21] Honglei Bai and Md Mahbub Alam. Dependence of square cylinder wake on reynolds number. *Physics of Fluids*, 30(1):015102, 2018.
- [22] Atul Sharma and V Eswaran. Heat and fluid flow across a square cylinder in the two-dimensional laminar flow regime. *Numerical Heat Transfer, Part A: Applications*, 45(3):247–269, 2004.
- [23] C Norberg. Pressure forces on a circular cylinder in cross flow. In *Bluff-Body Wakes, Dynamics and Instabilities*, pages 275–278. Springer, 1993.
- [24] Bijl Hester, Carpenter Mark H, and Vatsa Veer N. Time integration schemes for the unsteady navier-stokes equations. 2001.
- [25] Xia Ma and George Em Karniadakis. A low-dimensional model for simulating three-dimensional cylinder flow. *Journal of Fluid Mechanics*, 458:181–190, 2002.
- [26] BN Rajani, A Kandasamy, and Sekhar Majumdar. Numerical simulation of laminar flow past a circular cylinder. *Applied Mathematical Modelling*, 33(3):1228–1247, 2009.
- [27] N Ramos-García, H Sarlak, Søren Juhl Andersen, and Jens Nørkær Sørensen. Simulation of the flow past a circular cylinder using an unsteady panel method. *Applied Mathematical Modelling*, 44:206–222, 2017.
- [28] Bradford E Green, Ryan Czerwiec, Chris Cureton, Chad Lillian, Sergey Kernazhitskiy, Tim Eymann, Jason Torres, Keith Bergeron, and Robert Decker. Evaluation of flow solver accuracy using five simple unsteady validation cases. In *49th AIAA Aerospace Sciences Meeting*, pages 2011–0029, 2011.
- [29] CHK Williamson and A Roshko. Measurements of base pressure in the wake of a cylinder at low reynolds numbers. *Zeitschrift für Flugwissenschaften und Weltraumforschung*, 14:38–46, 1990.